Received: 3 August 2023 | Revised: 4 October 2023 | Accepted: 11 October 2023

DOI: 10.1002/JPER.23-0469

JOURNAL OF Periodontology

ORIGINAL ARTICLE

Superoxide dismutase 2 scavenges ROS to promote osteogenic differentiation of human periodontal ligament stem cells by regulating Smad3 in alveolar bone-defective rats

Wei Qiu[1] | **Qian Sun**[1] | **Na Li**[1] | **Zehao Chen**[1] | **Hongle Wu**[2] | **Zhao Chen**[1] | **Xiaolan Guo**[1] | **Fuchun Fang**[1]

[1]Department of Stomatology, Nanfang Hospital, Southern Medical University, Guangzhou, China

[2]Department of Endodontics, Stomatological Hospital, School of Stomatology, Southern Medical University, Guangzhou, China

Correspondence
Fuchun Fang, Department of Stomatology, Nanfang Hospital, Southern Medical University, 1838 Guangzhou Avenue North, Guangzhou 510515, China.
Email: fangfuchun@smu.edu.cn

Funding information
The National Nature Science Foundation of China, Grant/Award Numbers: 82170942, 82101024, 82100996; Natural Science Foundation of Guangdong Province, Grant/Award Numbers: 2020A1515110027, 2021A1515010854; Guangzhou Science and Technology Plan Project, Grant/Award Number: 2023A04J0426; Fundamental Research Project of the Shenzhen Science and Technology Innovation Committee, Grant/Award Number: JCYJ20210324121007020

Abstract

Background: Osteogenic differentiation of human periodontal ligament stem cells (hPDLSCs) is an essential event in alveolar bone regeneration. Oxidative stress may be the main inhibiting factor of hPDLSC osteogenesis. Superoxide dismutase 2 (SOD2) is a key antioxidant enzyme, but its effect on hPDLSC osteogenic differentiation is unclear.

Methods: Several surface markers were detected by flow cytometry, and the differentiation potential of hPDLSCs was validated by alkaline phosphatase (ALP), Alizarin Red S, and Oil Red O staining. Osteogenic indicators of hPDLSCs were detected by real-time quantitative polymerase chain reaction (RT-qPCR), Western blotting, and ALP staining. Furthermore, alveolar bone defect rat models were analyzed through micro-CT, hematoxylin and eosin, and Masson staining. The intracellular reactive oxygen species (ROS) level was evaluated by a ROS assay kit. Finally, the expression of SOD2, Smad3, and p-Smad3 in hPDLSCs was detected by RT-qPCR and Western blotting (WB).

Results: SOD2 positively regulated the gene and protein expressions of ALP, BMP6, and RUNX2 in hPDLSCs ($p < 0.05$). Ideal bone formation and continuous cortical bone were obtained by transplanting LV-SOD2 hPDLSCs (lentivirus vector for overexpressing SOD2 in hPDLSCs) in vivo. Exogenous H_2O_2 downregulated osteogenic indicators (ALP, BMP6, RUNX2) in hPDLSCs ($p < 0.05$); this was reversed by overexpression of SOD2. WB results showed that the Smad3 and p-Smad3 signaling pathways participated in the osteogenic process of SOD2 in hPDLSCs.

Conclusion: SOD2 positively regulated hPDLSC osteogenic differentiation in vitro and in vivo. Mechanistically, SOD2 promotes hPDLSC osteogenic differentiation by regulating the phosphorylation of Smad3 to scavenge ROS.

Wei Qiu, Qian Sun, and Na Li contributed equally to this article.

This work provides a theoretical basis for the treatment of alveolar bone regeneration.

KEYWORDS
bone regeneration, osteogenesis, reactive oxygen species, superoxide dismutase 2

1 | INTRODUCTION

Alveolar bone defects have attracted widespread attention worldwide.[1] Periodontitis, chronic apical periodontitis, trauma, tumor, and iatrogenic injuries can cause irreversible destruction and loss of alveolar bone, damaging the physiological function of people.[2] With the deepening of stem cell research and the development of materials, tissue engineering technology has provided new insights for bone regeneration.[3,4] Exploring suitable seed cells, evaluating the potential risks associated with transplanted cells, and selecting scaffolds or carriers are key to the current application of stem cells in alveolar bone regeneration.[5,6] Periodontal ligament stem cells (PDLSCs) are considered well-suited for alveolar bone regeneration.[7] PDLSCs have demonstrated proliferative and regenerative capacities in multiple studies,[8–11] making them an ideal source of stem cells for alveolar bone regeneration.

It has been reported that the osteogenic differentiation ability of human periodontal ligament stem cells (hPDLSCs) is impaired in an oxidative stress environment,[12] which may affect their role in tissue engineering. A growing body of research suggests that reactive oxygen species (ROS)-mediated oxidative stress is strongly associated with bone destruction during inflammation, such as that observed in rheumatoid arthritis, periodontitis, osteoporosis, and bone remodeling disorders in diabetes.[13–16] Previous studies have shown that ROS plays a regulatory role in the process of cellular osteogenic differentiation.[17] At high levels, the toxic effect of ROS hinders the process of osteogenic differentiation, while removing ROS enhances the osteogenic effect.[18,19] Therefore, it is inferred that regulating ROS levels during alveolar bone regeneration represents a critical step in osteogenesis.

As a member of the body's own antioxidant enzyme system, superoxide dismutase 2 (SOD2) can catalyze the disproportionation of superoxide radicals into hydrogen peroxide and molecular oxygen, representing the first line of mitochondrial defense against ROS.[20–22] Through tandem mass tag quantitative proteomic analysis, our team found that SOD2 showed the most significant upregulation during osteogenic differentiation of hPDLSCs in a time/differentiation state-dependent manner.[23] These results suggest that SOD2 plays a role in the osteogenic differentiation of hPDLSCs. However, no previous study has reported the ability of SOD2 to regulate osteogenic differentiation of hPDLSCs, and the specific mechanism of action requires further study.

In this study, we explored the effect of SOD2 on osteogenic differentiation of hPDLSCs through in vitro and in vivo experiments, with the aim to elucidate the underlying mechanism by which SOD2 regulates osteogenic differentiation of hPDLSCs and to provide a theoretical basis for promoting the treatment of alveolar bone regeneration.

2 | MATERIALS AND METHODS

2.1 | Isolation and culture of hPDLSCs

This study was approved by the Ethics Committee of Nanfang Hospital, Southern Medical University (NFEC-2021-031), and informed consent was obtained from the patients or their guardians in advance. hPDLSCs were obtained from periodontally healthy donors (aged 14–25 years; molars or premolars) who had requested tooth extraction for orthodontic treatment or impacted teeth at the Department of Stomatology, Nanfang Hospital, Southern Medical University. The periodontal ligament tissue was carefully scraped from the middle third of the root surface and cut into small pieces to approximately 1 mm3 per piece, before digesting with 3 mg/mL type I collagenase (Gibco, USA) for 20 min at 37°C. The obtained hPDLSCs were inoculated into a culture flask and maintained in Dulbecco's Modified Eagle Medium (DMEM; Gibco, USA) with 10% fetal bovine serum (FBS; Gibco, USA) and 1% penicillin/streptomycin (Gibco, USA). The medium was renewed every 3 days until the cell monolayer reached 80% confluency, at which point hPDLSCs were obtained using the limiting dilution method. hPDLSCs at Passages 3–6 were used for subsequent experiments.

2.2 | Identification of hPDLSCs by flow cytometry

The hPDLSCs obtained above were identified by flow cytometry. After rinsing with phosphate-buffered saline

(PBS) three times, 1×10^6 cells were resuspended in 50 μL PBS and then incubated with the conjugated antibody against mesenchymal surface marker antibodies (CD29, CD73, CD90, CD14, CD34, CD45) for 20 min on ice in the dark. Cells were identified by flow cytometry, and the obtained data were analyzed with MoFlo XDP software for flow cytometry (Beckman Coulter, USA).

2.3 | Induction of osteogenic and adipogenic differentiation

P3 hPDLSCs were seeded into 12-well plates (1×10^4 cells/cm^2). Upon reaching 70%–80% confluence, the medium was renewed with osteogenic or adipogenic induction medium for cell differentiation. For osteogenic differentiation, cells were incubated for 7 or 14 days in an osteogenic medium containing 10% FBS-DMEM (Gibco, USA) supplemented with 100 nM dexamethasone (Sigma-Merck, USA), 10 mM β-glycerophosphate (Sigma-Merck, USA), and 50 μg/mL L-ascorbic acid (Sigma-Merck, USA). The medium was refreshed every 3 days. After osteogenic induction, alkaline phosphatase (ALP) and Alizarin Red S (ARS) staining were used to evaluate osteogenic differentiation.

For adipogenic differentiation, after reaching 60%–70% confluence, the cells were incubated for 21 days with an adipogenic medium (Pythonbio, China), which was refreshed every 3 days. After adipogenic induction, Oil Red O staining was used to evaluate the effect of adipogenic differentiation.

2.4 | ALP, ARS, and Oil Red O staining

For ALP staining, after 7 days of osteogenesis induction, hPDLSCs were washed with PBS three times, fixed with 4% paraformaldehyde, and stained with BCIP/NBT Alkaline Phosphatase Color Development Kits (Beyotime, China) for 20 min at room temperature. Images were obtained using an IX73 microscope (Olympus, Japan).

For ARS staining, following 14-day osteogenic induction, hPDLSCs were washed three times with PBS, fixed in 4% paraformaldehyde, and immersed in 2% ARS solution (pH = 4.2, Leagene, China) for 15 min at room temperature. Images were obtained using an Olympus IX73 microscope.

For Oil Red O staining, after 21 days of adipocyte differentiation, hPDLSCs were washed three times with distilled water, fixed in 4% paraformaldehyde for 20 min, stained with Modified Oil Red O solution (C0158S-1, Beyotime, China) for 30 min, and then washed a further three times with distilled water. Images were obtained using an Olympus IX73 microscope.

2.5 | Construction and transfection of lentiviral vectors

The lentivirus vector for overexpressing SOD2 (LV-SOD2) and the corresponding negative control lentivirus (LV-Vector) were constructed by Genechem (Genechem, China). P3 hPDLSCs were seeded into a 12-well plate at a density of 1×10^4 cells/well before being transfected with Lv-SOD2 and LV-Vector at a multiplicity of infection (MOI) of 50 in the presence of 5 μg/mL polybrene. The transfection procedure was performed according to the manufacturer's instructions. The transfection efficiency was verified by real-time quantitative polymerase chain reaction (RT-qPCR) and Western blotting (WB) after 72 h of transfection.

2.6 | Small interfering RNA transfection

SOD2 small interfering RNA (siRNA) was purchased from RiboBio (RiboBio, China). Briefly, P3 hPDLSCs were seeded into a 12-well plate at a density of 5×10^4 cells/well, and transfection was performed using a riboFECT CP transfection kit (cat# C10511-05; RiboBio, China) according to the manufacturer's instructions. Negative control siRNA (si-NC) with a nonsense sequence was used as the negative control. The siRNA sequences used are shown in Table S1 in the online *Journal of Periodontology*. Knockdown efficiency was evaluated by RT-qPCR and WB.

2.7 | Real-time quantitative PCR

Total cellular RNA was extracted with an EZ-press RNA Purification Kit (EZBioscience, USA). Total RNA quantification was performed using a NanoDrop 2000 (Thermo Fisher Science, China), and reverse transcription was conducted using a Color Reverse Transcription Kit (EZBioscience, USA). Subsequent RT-qPCR was performed using MagicSYBR Mixture Kits (Kangwei Century, China) on a Quant-Studio 6 system. The primer sequences used are shown in Table S1.

2.8 | Western blotting

Protein was extracted from hPDLSCs using radioimmunoprecipitation assay (RIPA) buffer (Beyotime, China) containing 1% protease inhibitor. The concentration of lysate proteins was quantified using a bicinchoninic acid (BCA) protein assay kit (Beyotime, China). The prepared protein samples were loaded onto 10% SDS-PAGE gel, followed by transfer onto a 0.45-μm polyvinylidene

difluoride (PVDF) membrane (Millipore, USA). The membrane was immersed in 1X Protein Free Rapid Blocking Buffer (Epizyme, China) for 15 min, before incubating with primary antibodies against SOD2 (24127-1-AP; Proteintech, USA), ALP (ab224335; Abcam, USA), RUNX2 (YT5356; Immunoway, USA), BMP6 (ab155963; Abcam, USA), GAPDH (10494-1-AP; Proteintech, USA), Smad3 (ab40854; Abcam, USA), and p-Smad3 (ab52903; Abcam, USA) at 4°C overnight. Following incubation, HRP-conjugated AffiniPure IgG secondary antibody (SA00001-2, goat anti-rabbit and SA00001-1, goat anti-mouse; Proteintech, USA) was added and incubated for 1 h at room temperature. The membranes were visualized and exposed to enhanced chemiluminescence reagents (cat#BL520B; Biosharp Life Sciences, China) and analyzed with an image analyzer (BLT GelView 6000 Pro), before measuring the relative density of the bands with ImageJ 5.0 (NIH, USA).

2.9 | Establishment of alveolar bone defect model

We successfully constructed a rat alveolar bone defect model referring to the research of Yang et al.[24] As shown in Figure 3A, 7-week-old male Sprague–Dawley (SD) rats (weight range 250 ± 20 g) were provided by the Animal Center of Southern Medical University. The animals were housed under specific pathogen-free conditions (22 ± 2°C; 55% ± 10% humidity) under a 12/12 h light–dark cycle. All animal experiments were approved by the Animal Centre and Use Committee of Nanfang Hospital, Southern Medical University (IACUC-LAC-20220916-004) and conducted strictly according to the experimental protocol. After 1 week of acclimation, the rats were placed under general anesthesia with 1% pentobarbital sodium (40 mg/kg). A medical incision was made on the mesial of the maxillary first molar to expose the mesial root and alveolar bone of the maxillary first molar. Next, the rats underwent surgery to create left maxillary alveolar bone defects (1.5 mm in width, 1.5 mm in depth, and 3 mm in length). All rats were randomly divided into the following four groups ($n = 3$): (1) control group, in which the defect area was not filled and the wound was directly sutured; (2) biphasic calcium phosphate (BCP)+hPDLSCs group, in which the bone defect was filled with BCP particles mixed with untreated hPDLSCs; (3) BCP+LV-Vector hPDLSCs group, in which the bone defect was filled with BCP particles mixed with hPDLSCs transfected with LV-Vector; and (4) BCP+LV-SOD2 hPDLSCs group, in which the bone defect was filled with BCP particles mixed with hPDLSCs transfected with SOD2-overexpressing lentivirus. The mixture of cells and BCP materials was adsorbed with a gelatin sponge before being used to fill the bone defect to avoid diffusion and displacement of the granular material in the early stage after implantation. After surgery, all rats were fed a normal diet and provided water, and the wound healing and systemic condition of the rats were observed the next day. After 4 weeks, the rats were sacrificed by carbon dioxide inhalation, and the left maxillary alveolar bones were collected. All samples were fixed with 4% paraformaldehyde at 4°C for 24 h.

2.10 | Micro-CT

The maxillae samples ($n = 3$) were scanned using a micro-CT scanner (kyScan 1276; Bruker, Belgium) at a current of 200 μA and voltage of 100 kV, with an isometric pixel size of 10 μm. Alveolar bone trabecular analysis was performed surrounding the mesial of the mesial root of the maxillary first molar, 1.5 mm in width, 1.5 mm in depth, and 3 mm in length as a region of interest (ROI). SkyScan CTAn software (version 1.20.3.0; Bruker, Belgium) was used to obtain 3D images to reconstruct the ROI and to calculate the trabecular thickness (Tb.Th), trabecular number (Tb.N), trabecular separation (Tb.Sp), and the relative trabecular bone volume (bone volume [BV]/tissue volume [TV]).

2.11 | Histological analysis

The tissue was decalcified with 14% EDTA for 4 weeks, before dehydration in a gradient series of alcohol and embedding in paraffin. Subsequently, the paraffin tissue blocks were sectioned in the sagittal direction along the mesial of the first molars at a thickness of 4 μm. Then, for histological analysis, the sections were subjected to hematoxylin and eosin (HE) and Masson staining to visualize defect healing and bone formation. The Masson staining kit (GP1137) was purchased from Servicebio (China).

2.12 | Measurement of intracellular ROS

The ROS content of hPDLSCs was determined using a Reactive Oxygen Species Assay Kit (Beyotime, China). DCFH-DA was prediluted using a serum-free cell culture medium at a ratio of 1:1000. hPDLSCs were seeded into 12-well plates at a density of 5×10^4 cells/well, before adding DCFH-DA solution to completely cover the adherent cells. Following incubation for 20 min at 37°C, the ROS levels in the hPDLSCs were assessed by a fluorescence microscope.

2.13 | Cell Counting Kit-8

The Cell Counting Kit-8 (CCK-8) assay (Beyotime, China) was employed to determine the effect of H_2O_2 concentration on the viability of hPDLSCs. Briefly, hPDLSCs were plated into 96-well plates and various concentrations of H_2O_2 (25, 50, 100, 200 nM) were added and cultivated for 48 h. Then, CCK-8 solution (10 μL) was added into each well and cultured for another 2 h. Finally, the optical density was determined at 450 nm using a microplate reader.

2.14 | Statistical analysis

GraphPad Prism software version 8.0.1 (San Diego, California, USA) was used to conduct statistical analysis. All data are represented as the mean ± standard error of the mean (SEM). Since the data achieved normality, Student's *t* test was used for comparisons of two independent groups, and one-way analyses of variance (ANOVA) with Tukey's Honest Significant Difference (HSD) post hoc test and multiple comparisons were used to analyze differences in data from more than two groups. Differences were considered significant when $p < 0.05$ ($n = 3$).

3 | RESULTS

3.1 | Isolation, culture, and identification of hPDLSCs

Microscopically, cells with a typical fibroblast-like long spindle-shaped morphology crawled out along the edge of human periodontal ligament tissue, termed hPDLSCs (see Figure S1A in online *Journal of Periodontology*). After subculturing, cells grew in a vortex arrangement. Clonal colony experiments were performed on single cells obtained from dilution isolation, which showed that they grew in a clonal colony-like manner (see Figure S1A in online *Journal of Periodontology*). Flow cytometry analysis showed that hPDLSCs were positive for mesenchymal stem cell (MSC) markers CD29, CD73, and CD90 and negative for the monocyte marker CD14 and hematopoietic markers CD34 and CD45 (see Figure S1B in *Journal of Periodontology*). ALP staining, ARS staining, and Oil Red O staining were performed to evaluate the differentiation ability of hPDLSCs. The results showed that the isolated hPDLSCs had osteogenic and adipogenic differentiation capabilities (see Figure S1C–E in online *Journal of Periodontology*). In summary, the isolated hPDLSCs were mesenchymal-derived pluripotent stem cells.

3.2 | SOD2 improved osteogenic differentiation of hPDLSCs in vitro

To evaluate the effect of SOD2 on the osteogenic differentiation of hPDLSCs, we knocked down and overexpressed SOD2 in hPDLSCs. For subsequent experiments, we selected siRNA (si1-100 nmol) with the best interference efficiency and verified its effect using RT-qPCR and WB (Figure 1A–C). Furthermore, we selected a vector with an MOI value of 50 as an overexpression vector for the transfection of hPDLSCs and verified its effect using RT-qPCR and WB (Figure 2A–D). Next, we compared the gene expression of ALP, RUNX2, and BMP6 in hPDLSCs with or without osteogenic differentiation. Compared with the control group, the expression of osteogenesis-related genes was significantly increased in the osteogenic-induced medium (OM) group, indicating successful establishment of the osteogenic model of hPDLSCs. After knocking down SOD2 expression in hPDLSCs, the expression of osteogenesis-related genes (ALP, BMP6, RUNX2) in the si-SOD2 group was significantly downregulated compared with that in the OM+si-NC group ($p < 0.05$) (Figure 1D). However, when SOD2 was overexpressed in hPDLSCs, the expression of ALP, BMP6, and RUNX2 was significantly upregulated in the OM+LV-SOD2 group compared with that in the OM+LV-Vector group (Figure 2E). The expression of proteins showed the same trend (Figures 1E,F and 2F,G). The results of ALP staining demonstrated that compared with the OM+si-NC group, ALP activity was significantly inhibited in hPDLSCs following the inhibition of SOD2 (Figure 1G). Nevertheless, the overexpression of SOD2 could enhance the ALP activity of hPDLSCs (Figure 2H). Taken together, these results suggested that SOD2 participated in and positively regulated the osteogenic differentiation of hPDLSCs.

3.3 | Transplantation of LV-SOD2 hPDLSCs promoted bone regeneration in alveolar bone defect rats

Four weeks after surgery, micro-CT scanning and 3D reconstruction of the rat maxilla were performed to assess osteogenesis. As shown in Figure 3B, on the coronal plane, varying degrees of new bone formation were seen in the remaining three groups compared with the control group. We noted no significant difference between the BCP+hPDLSCs and BCP+LV-Vector hPDLSCs groups, while the area of bone defects in the BCP+LV-SOD2 hPDLSCs group decreased most significantly compared with that in the other groups. On the sagittal plane, new bone formation on the root surface of the first

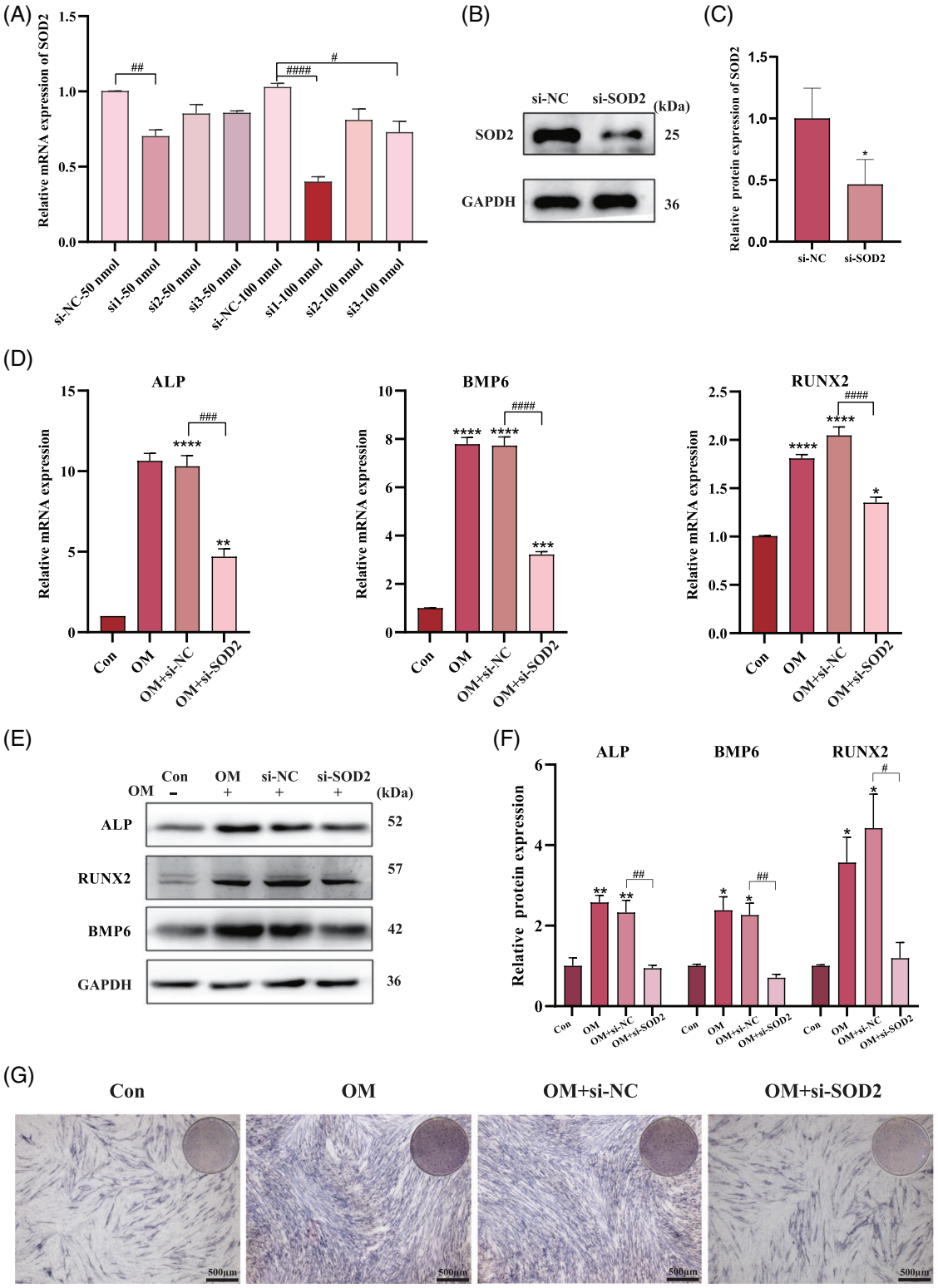

FIGURE 1 Knocking down SOD2 inhibits osteogenesis of hPDLSCs. (A–C) Efficacy of inhibition of SOD2 by siRNA was measured by RT-qPCR and Western blot. (D) Transcript level of osteo-specific markers, including ALP, BMP6, and RUNX2, in Con, OM, OM+si-NC, and OM+si-SOD2 groups. (E, F) Protein expression of osteo-specific markers and quantitative analysis of above groups. (G) ALP staining after osteogenic induction for 7 days. Data are expressed as mean ± standard error of the mean (SEM) of three biologically independent experiments. ALP, alkaline phosphatase; Con, medium control; hPDLSCs, human periodontal ligament stem cells; OM, osteogenic-induced medium; RT-qPCR, real-time quantitative polymerase chain reaction; si-NC, negative control siRNA; siRNA, small interfering RNA; si-SOD2, siRNA-targeting SOD2; SOD2, superoxide dismutase 2. * represents comparison to control group and # represents comparison between the two groups. *p, #$p < 0.05$; **p, ##$p < 0.01$; ***p, ###$p < 0.001$; ****p, ####$p < 0.0001$.

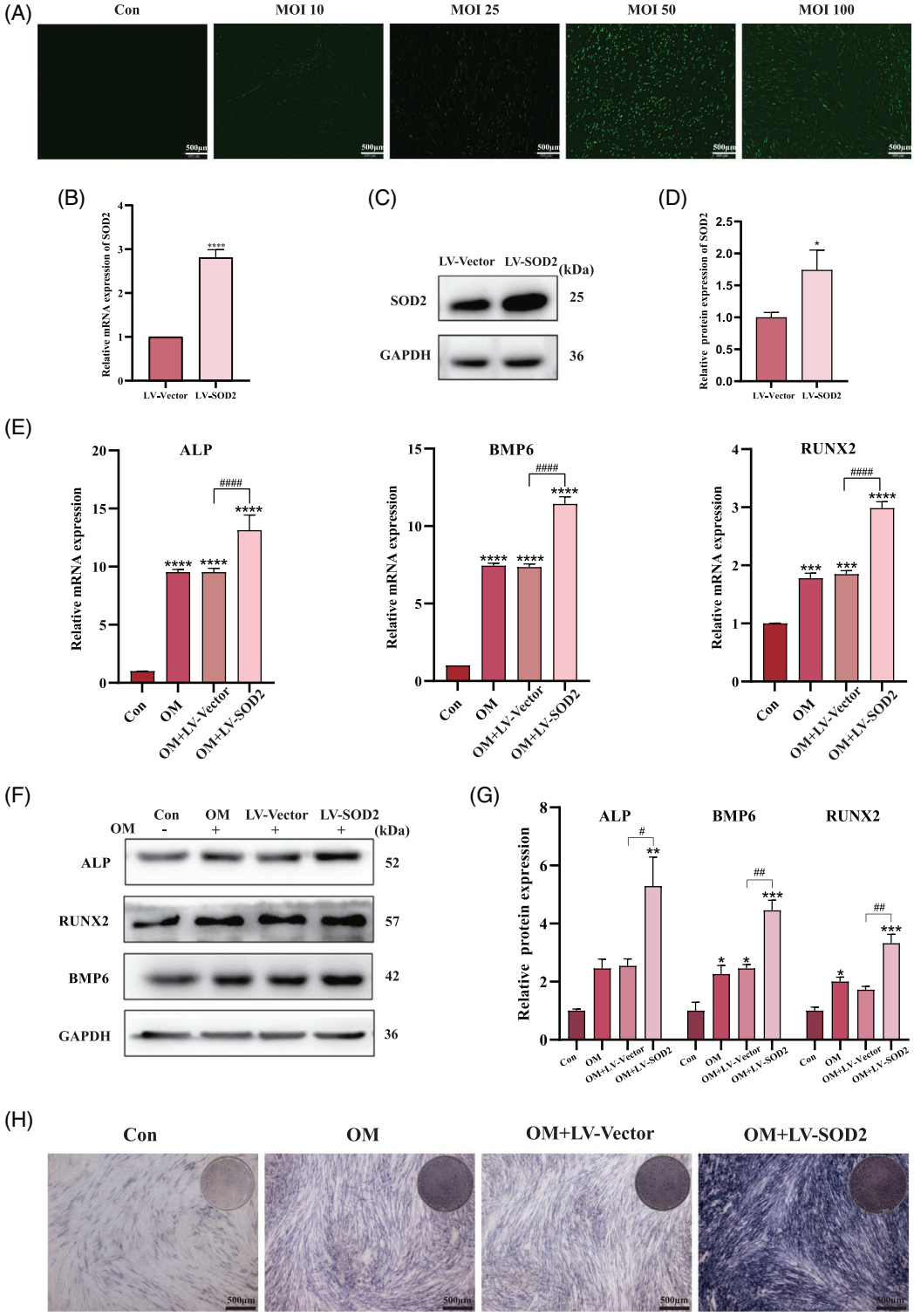

FIGURE 2 Overexpressed SOD2 improved osteogenesis of hPDLSCs. (A) Transfection with different MOI of LV-SOD2 in hPDLSCs. (B) Transcript level of SOD2 under MOI = 50 transfection condition. (C, D) SOD2 protein level and quantitative analysis under MOI = 50 transfection condition. (E) mRNA expression of osteo-specific markers including ALP, BMP6, RUNX2 in Con, OM, OM+LV-Vector, OM+LV-SOD2 groups. (F, G) Protein expression of osteo-specific markers and quantitative analysis of above groups. (H) ALP staining after osteogenic induction for 7 days. Data are expressed as mean ± standard error of the mean (SEM) of three biologically independent experiments. ALP, alkaline phosphatase; Con, medium control; hPDLSCs, human periodontal ligament stem cells; LV-SOD2, lentivirus vector for overexpressing SOD2; LV-Vector, negative control lentivirus; MOI, multiplicity of infection; OM, osteogenic-induced medium; SOD2, superoxide dismutase 2. * represents comparison to control group and # represents comparison between the two groups. *p, $^{\#}p < 0.05$; **p, ##$p < 0.01$; ***$p < 0.001$; ****p, $^{\#\#\#\#}p < 0.0001$.

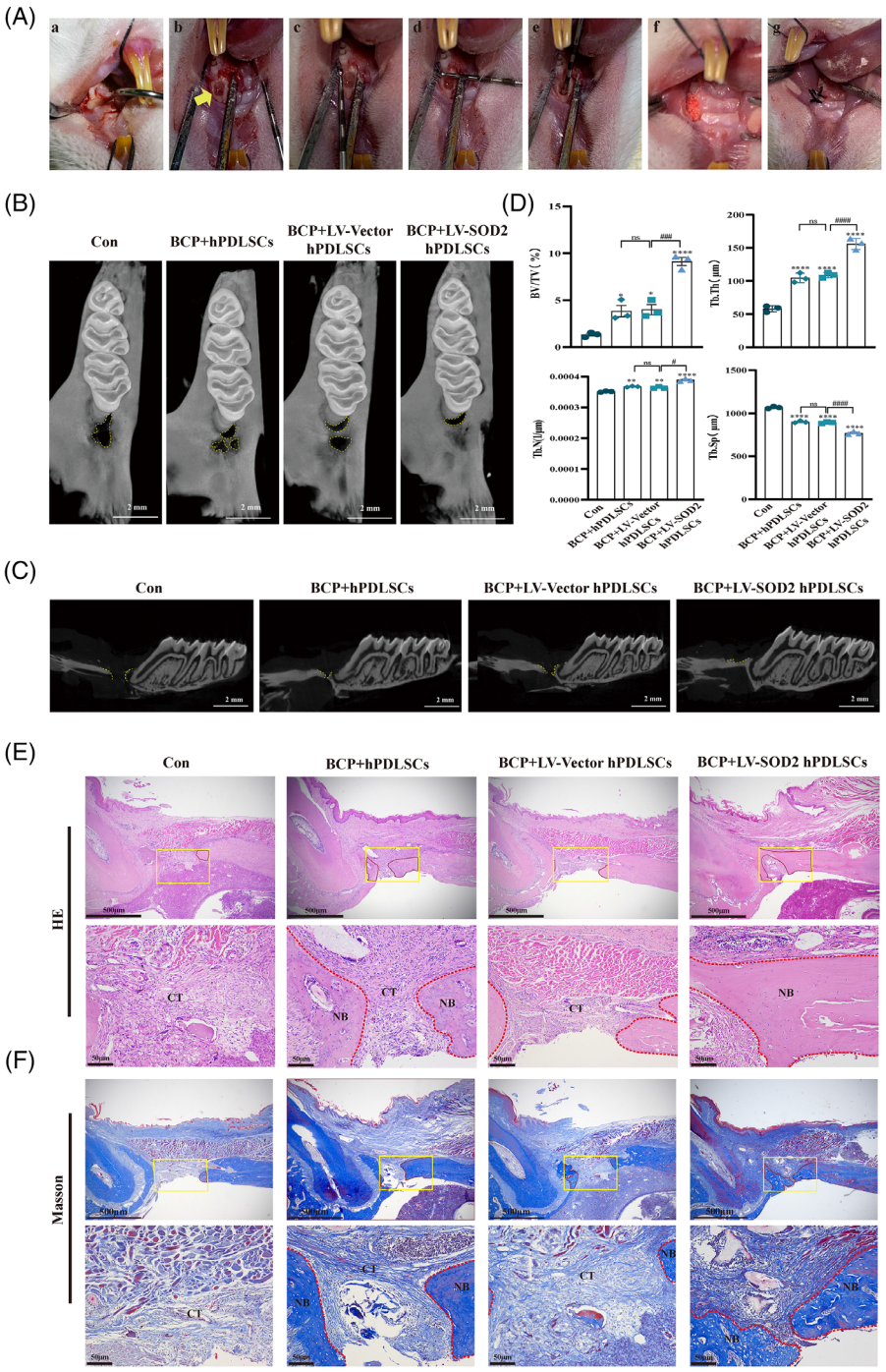

FIGURE 3 Micro-CT and histological assessment of alveolar bone regeneration in rats. (A) Process of establishing alveolar bone defect model. Medical incision was performed to expose alveolar bone of maxillary first molar (a). Bone defect creation on mesial surface of first molar (yellow arrow) (b). Each defect was 1.5 mm in width, 1.5 mm in depth, and 3 mm in length (c–e). Defect was filled with mixture of cells and materials, before stitching the wound closed (f, g). (B, C) Micro-CT images showing coronal (B) and sagittal (C) views of maxillary alveolar bone defect areas of rats in Ctrl, BCP+hPDLSCs, BCP+LV-Vector hPDLSCs, and BCP+LV-SOD2 hPDLSCs groups (yellow dotted lines show edge of alveolar bone defects). (D) Quantitative analysis of micro-CT, including trabecular thickness (Tb.Th), trabecular number (Tb.N), trabecular separation (Tb.Sp), and relative trabecular bone volume (bone volume [BV]/tissue volume [TV]). (E, F) Histological analysis of bone defect areas through HE staining (E) and Masson staining (F) (yellow rectangular boxes represent area of bone defect, and area with solid red lines and red dotted lines is new bone). Data are expressed as mean ± standard error of the mean (SEM) of three biologically independent experiments. BCP, biphasic calcium phosphate; Con, medium control; CT, connective tissue; Ctrl, control; HE, hematoxylin and eosin; hPDLSCs, human periodontal ligament stem cells; LV-SOD2, lentivirus vector for overexpressing SOD2; LV-Vector, negative control lentivirus; NB, newly formed bone; ns, nonsignificant; SOD2, superoxide dismutase 2. * represents comparison to control group and $^{\#}$represents comparison between the two groups. *p, #$p < 0.05$; **p, $^{\#\#\#}p < 0.001$; ****p, $^{\#\#\#\#}p < 0.0001$.

molars was observed in all three groups except the control group, among which the BCP+LV-SOD2 hPDLSCs group exhibited the best bone regeneration effect, with clear and continuous cortical bones observed to wrap around the tooth root (Figure 3C). ROI quantitative analysis showed that compared with other groups, the bone volume fraction (BV/TV), Tb.N, Tb.Th, and Tb.Sp were significantly increased in the BCP+LV-SOD2 hPDLSCs group ($p < 0.05$) (Figure 3D), indicating that the SOD2 overexpression group had the best repair effect of alveolar bone defects.

The results of HE and Masson staining showed that compared with the control group, different degrees of histological healing occurred in the remaining three groups, among which the BCP+hPDLSCs group and BCPLV-Vector hPDLSCs group mainly exhibited connective tissue epithelial healing, while the defect area was mainly disordered collagen fibers with a small amount of new bone formation. By contrast, the BCP+LV-SOD2 hPDLSCs groups showed increased formation of new bone (Figure 3E,F). The above findings jointly illustrate the promoting effect of SOD2 on alveolar bone regeneration in vivo.

3.4 | Overexpression of SOD2 reversed inhibition of hPDLSC osteogenesis by exogenous H_2O_2

We next employed a ROS probe to evaluate the effect of SOD2 on intracellular ROS levels of osteogenic differentiated hPDLSCs. As shown in Figure 4A, the ROS level of osteogenic differentiated hPDLSCs was significantly reduced compared with that of the control group, indicating that osteogenic differentiation of hPDLSCs was conducted in a relatively low ROS environment. After inhibiting the SOD2 expression of hPDLSCs, the ROS level increased significantly, which, combined with the results of 3.1 and 3.2, suggests that SOD2 promotes the osteogenic differentiation of hPDLSCs by scavenging ROS in hPDLSCs. Therefore, we added exogenous H_2O_2 during osteogenic differentiation of hPDLSCs to verify this hypothesis. The results showed that compared with the OM group, the osteogenesis-related gene expression level and protein level of the OM+H_2O_2 group were statistically significantly inhibited ($p < 0.05$), but the osteogenic effect in the OM+LV-SOD2+H_2O_2 group was significantly enhanced ($p < 0.05$) (Figure 4B–D), indicating that overexpression of SOD2 could reverse the inhibitory effect of H_2O_2 on the osteogenic differentiation of hPDLSCs. ALP staining showed a similar trend with the results of RT-qPCR and WB (Figure 4E).

3.5 | Smad3 is involved in SOD2-mediated regulation of H_2O_2-treated hPDLSC osteogenesis

Subsequently, we examined the expression of related signal pathway proteins by WB and observed that the levels of Smad3 and p-Smad3 were significantly reduced after interference with SOD2 expression ($p < 0.05$) (Figure 5A,B). By contrast, when the expression of SOD2 was upregulated, the expression of Smad3 and p-Smad3 also increased (Figure 5C,D), suggesting that SOD2 could positively regulate the level of Smad3 in hPDLSCs and activate its phosphorylation, thereby promoting osteogenesis. In addition, WB analysis demonstrated that the expression levels of Smad3 and p-Smad3 decreased significantly in hPDLSCs following treatment with exogenous H_2O_2, which showed that H_2O_2 could inhibit the expression of Smad3 and its phosphorylation in hPDLSCs (Figure 5E,F). These results indicated that Smad3 may participate in the SOD2-mediated promotion of osteogenic differentiation in H_2O_2-treated hPDLSCs.

4 | DISCUSSION

In this study, we confirmed that SOD2 regulates osteogenesis of hPDLSCs in vitro. Overexpression of SOD2 significantly upregulated osteogenesis indicators, which is consistent with previous studies on SOD2 in bone regulation.[23] Kim et al. inhibited or overexpressed SOD2 in osteoclasts and found that SOD2 controlled osteoclastic formation.[25] In vivo, Schoppa et al. and Kobayashi et al. established mouse models of osteoblast or osteocyte-specific SOD2 deficiency and found significant bone loss in trabecular and cortical bone, which was accompanied by decreased osteoblast or osteocyte activity, inhibition of bone formation, and increased bone resorption.[26,27] In line with this, in the present study, we concluded that SOD2 promoted osteogenic differentiation of hPDLSCs in vivo. More bone formation and continuous cortical formation were observed in the BCP+LV-SOD2 hPDLSCs group compared with the control, BCP+hPDLSCs, and BCP+LV-Vector hPDLSCs groups.

SOD2 functions to directly catalyze O_2^- to H_2O_2, before further catalyzing to H_2O and O_2 by catalase.[28,29] We detected ROS levels in hPDLSCs using a ROS probe and found that relative to the undifferentiated group, the ROS levels decreased significantly during osteogenic differentiation of hPDLSCs, which was consistent with the work of Chen et al. in MSCs.[30] Moreover, the ROS levels within hPDLSCs were elevated after the inhibition of SOD2 in osteogenic differentiation. From this, we

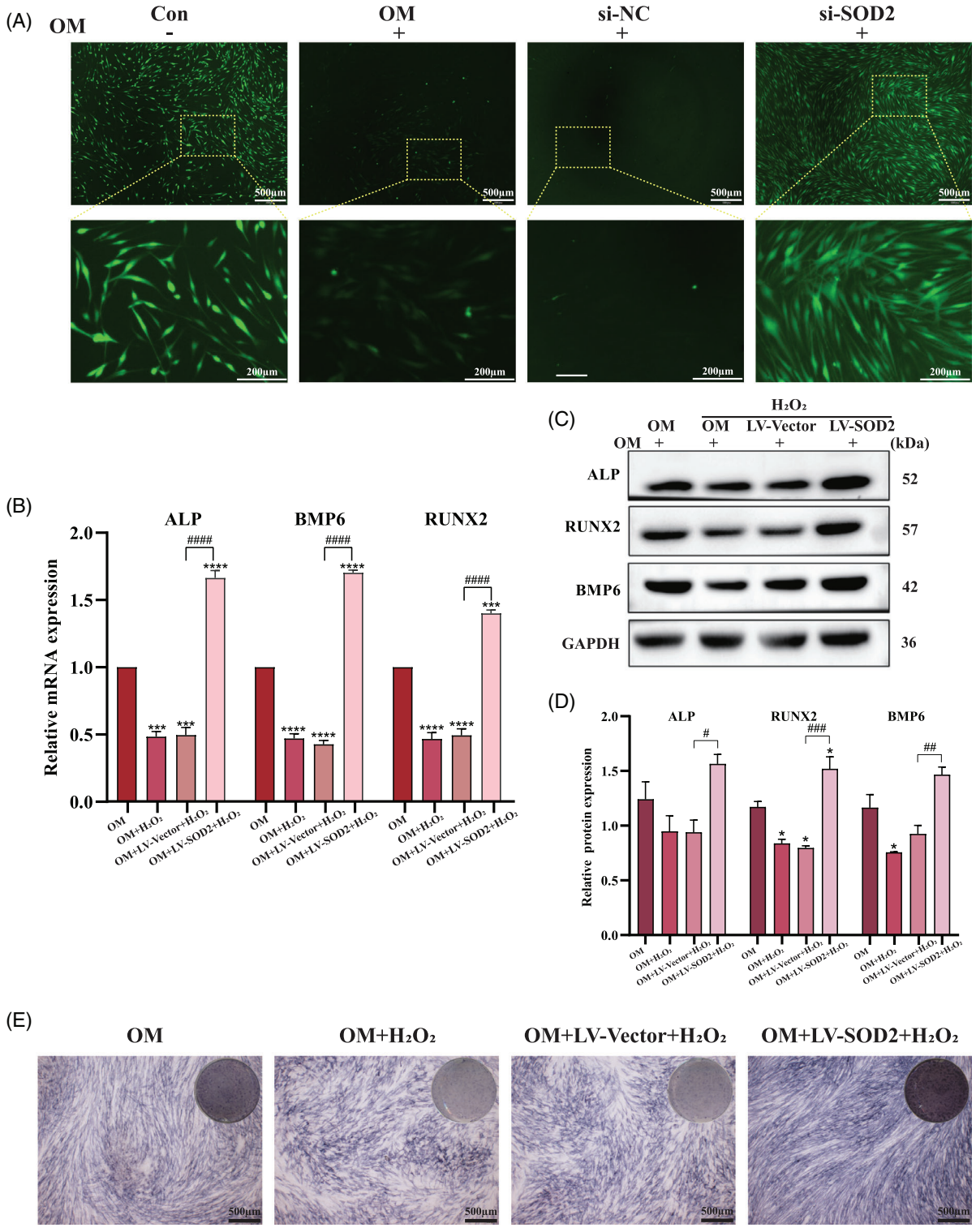

FIGURE 4 Overexpression of SOD2 reversed inhibition of hPDLSC osteogenesis by exogenous H_2O_2. (A) Detection of intracellular ROS levels in Con, OM, OM+si-NC, and OM+si-SOD2 groups. Green fluorescence reflects intracellular ROS. (B) Impact of addition of exogenous H_2O_2 on osteo-specific markers (ALP, BMP6, RUNX2) of hPDLSCs by RT-qPCR. (C, D) Impact of addition of exogenous H_2O_2 on osteo-specific markers of hPDLSCs by Western blotting. (E) ALP staining after osteogenic induction for 7 days. Data are expressed as mean ± standard error of the mean (SEM) of three biologically independent experiments. ALP, alkaline phosphatase; Con, medium control; hPDLSC, human periodontal ligament stem cell; LV-SOD2, lentivirus vector for overexpressing SOD2; LV-Vector, negative control lentivirus; OM, osteogenic-induced medium; ROS, reactive oxygen species; RT-qPCR, real-time quantitative polymerase chain reaction; si-NC, negative control siRNA; siRNA, small interfering RNA; si-SOD2, siRNA-targeting SOD2; SOD2, superoxide dismutase 2. *represents comparison to control group and # represents comparison between the two groups. *p, $^{\#}p < 0.05$; $^{\#\#}p < 0.01$; ***p, $^{\#\#\#}p < 0.001$; ****p, $^{\#\#\#\#}p < 0.0001$.

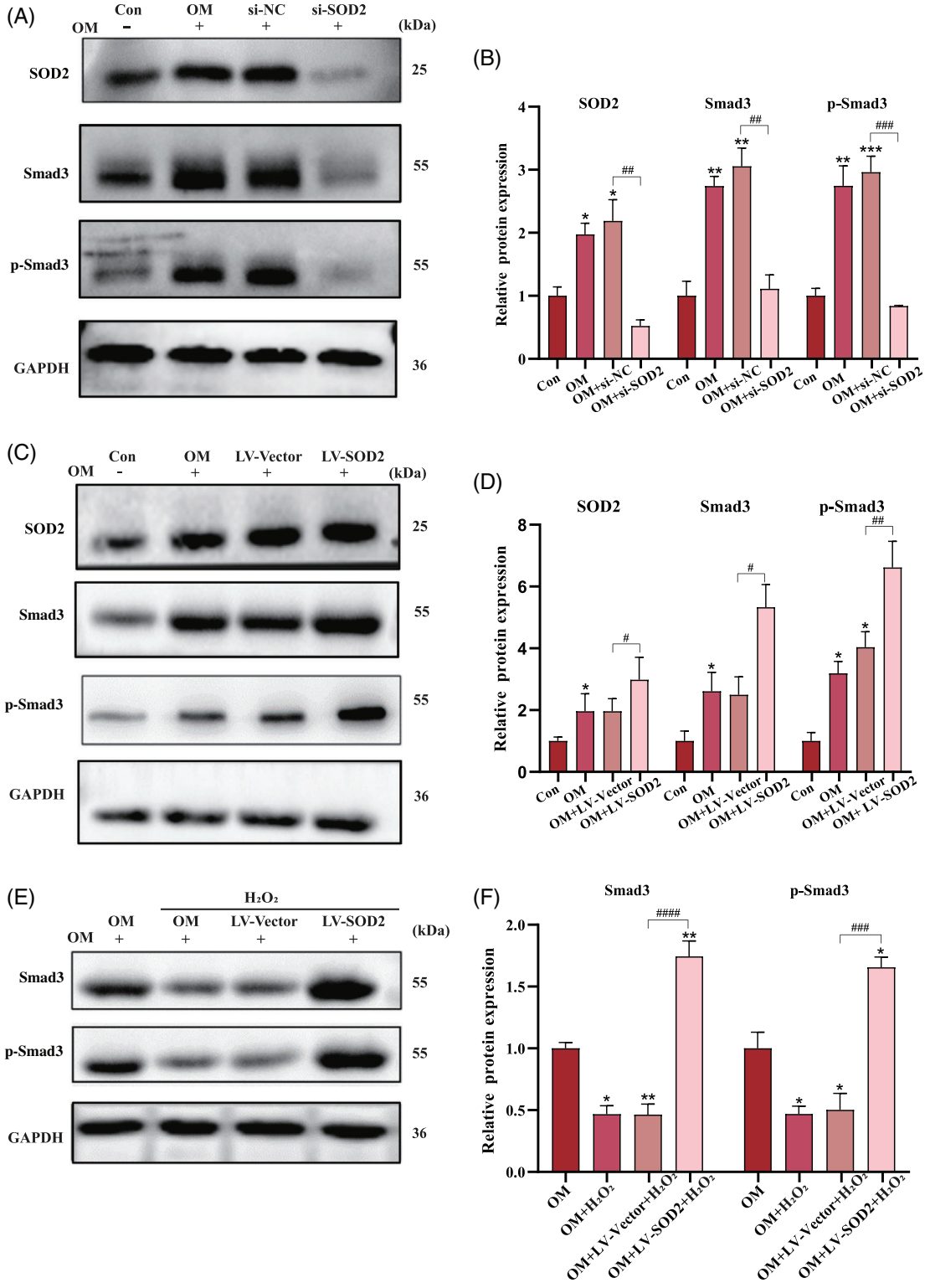

FIGURE 5 Smad3 is involved in SOD2-mediated regulation of H_2O_2-treated hPDLSC osteogenesis. (A, B) Protein expression of SOD2, Smad3, and p-Smad3 following transfection of hPDLSCs with si-SOD2 and quantitative analysis. (C, D) Expression of SOD2, Smad3, and p-Smad3 protein following SOD2 overexpression and quantitative analysis. (E, F) Impact of exogenous H_2O_2 on protein expression of Smad3 and p-Smad3 and quantitative analysis. Data are expressed as mean ± standard error of the mean (SEM) of three biologically independent experiments. Con, medium control; hPDLSC, human periodontal ligament stem cell; LV-SOD2, lentivirus vector for overexpressing SOD2; LV-Vector, negative control lentivirus; OM, osteogenic-induced medium; si-NC, negative control siRNA; siRNA, small interfering RNA; si-SOD2, siRNA-targeting SOD2; SOD2, superoxide dismutase 2. * represents comparison to control group and # represents comparison between the two groups. *p, #p < 0.05; **p, ##p < 0.01; ***p, ###p < 0.001; ####p < 0.0001.

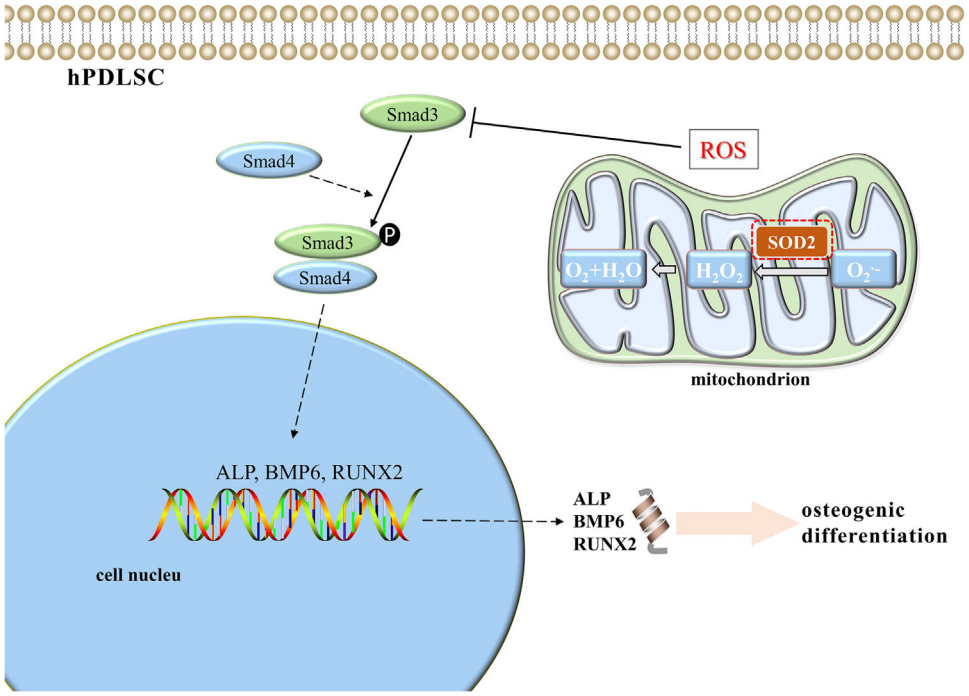

FIGURE 6 Schematic diagrams showing mechanism by which SOD2 promotes osteogenic differentiation of hPDLSCs. SOD2 scavenges intracellular ROS (including by promoting rapid decrease in H_2O_2 levels), thereby promoting Smad3 expression and its phosphorylation, which in turn causes osteogenic differentiation of hPDLSCs (increase in osteogenic-related factors). ALP, alkaline phosphatase; hPDLSCs, human periodontal ligament stem cells; ROS, reactive oxygen species; SOD2, superoxide dismutase 2.

speculated that SOD2 promoted osteogenic differentiation of hPDLSCs by scavenging intracellular ROS. To test this hypothesis, we added exogenous H_2O_2 to induce oxidative stress during osteogenic differentiation of hPDLSCs. We selected relatively high H_2O_2 concentrations (100 nM) that did not affect the proliferative activity of hPDLSCs and examined their effect on the osteogenic function of hPDLSCs.[31] The results suggested that H_2O_2 also inhibited the osteogenic function of hPDLSCs, and osteogenesis was significantly inhibited in the OM+H_2O_2 group and OM+LV-Vector+H_2O_2 group and significantly promoted in the OM+LV-SOD2+H_2O_2 group. The above findings indicated that SOD2 promoted osteogenic differentiation of hPDLSCs by regulating oxidative stress.

The entire osteogenic differentiation process is controlled by a variety of key targets, both at the transcriptional level and via extracellular signaling pathways, while the regulatory effect of RUNX2 on osteogenic differentiation in MSCs has been clarified previously.[32,33] RUNX2 is regulated by various pathways, with the transforming growth factor beta (TGF-β)/Smad pathway being one of the most important.[34] The Smad pathway plays an important role in cellular osteogenesis, and only Smad3 is closely related to osteogenic differentiation in the Smad family.[35] Inhibition of Smad3 phosphorylation reduces RANKL-induced ROS production, thereby preventing osteoclast differentiation and maturation.[36] Studies have found that after the treatment of osteoblasts with copper chloride, total SOD activity is inhibited and ROS is overproduced, which affects the activity of the TGF-β1/Smad3 pathway in osteoblasts.[37] However, no previous study has investigated whether there is a regulatory relationship between Smad 3 and SOD2, a key regulator of oxidative stress, in the context of osteogenic differentiation. We found that when the SOD2 expression of hPDLSCs was inhibited, Smad3 protein expression decreased, and when SOD2 was overexpressed, Smad3 protein expression also increased, suggesting that SOD2 positively regulates Smad3 protein levels. Furthermore, the addition of H_2O_2 alone triggered a similar change, indicating that Smad3 is also affected by H_2O_2. Therefore, we speculate that SOD2 may promote the overall clearance of intracellular ROS, thereby promoting the increase in Smad3 expression and its phosphorylation, which in turn leads to an increase in the level of osteogenic correlated factors and ultimately promotes the osteogenic differentiation of hPDLSCs.

In addition, we achieved better bone formation upon the transplantation of hPDLSCs that overexpressed SOD2 in alveolar bone-defective rats, and the mechanism of this MSC therapy is also worth discussing. Differentiation of MSCs is thought to play a definitive role only when they are transplanted in situ along with biomaterial to regenerate bone defects.[38–40] However, there is

currently controversy over the mechanism of homing and differentiation of MSCs after transplantation. A study in rats showed that MSCs survived for no more than 2 days after local injection.[41] Conversely, Yu et al. visualized the local injection of MSCs into the bladder of mice, and the number of cells disappeared on Day 28 after maintaining a certain number.[42] ROS-induced oxidative stress is one of the leading causes of MSC mortality after engraftment.[43] In our experiments, overexpression of SOD2 may have more hPDLSC survival and osteogenic differentiation due to increased resistance to oxidative stress, resulting in better therapeutic outcomes. However, this is only a speculation based on theory and results. In this paper, we focus on the mechanism by which SOD2 promotes osteogenic differentiation of hPDLSCs, and the mechanism of hPDLSC transplantation may have more influencing factors, which are not the focus of research here.

5 | CONCLUSION

In summary, we demonstrate that high levels of ROS could inhibit the osteogenic differentiation of hPDLSCs and that SOD2 positively regulated hPDLSC osteogenesis by scavenging ROS, especially H_2O_2. Preliminary mechanistic studies suggested that Smad3 acts as a downstream signal of SOD2 and is involved in undoing the osteogenic differentiation inhibition of hPDLSCs induced by ROS accumulation (Figure 6).

AUTHOR CONTRIBUTIONS

Wei Qiu and Fuchun Fang were responsible for experimental design, manuscript revision, and financial support. Qian Sun and Na Li contributed to data acquisition, analysis, and interpretation and drafted the manuscript. Zehao Chen and Xiaolan Guo contributed partly to data acquisition and analysis. Hongle Wu and Zhao Chen contributed to critically revising the manuscript and financial support. All authors gave final approval and agreed to be accountable for all aspects of the work, ensuring integrity and accuracy.

ACKNOWLEDGMENTS

This work was supported by grants from the National Nature Science Foundation of China (~~82170942~~ to F.F., 82101024 to W.Q., and 82100996 to Z.C.), the Natural Science Foundation of Guangdong Province (2020A1515110027 to W.Q. and 2021A1515010854 to F.F.), the Guangzhou Science and Technology Plan Project (2023A04J0426 to H.W.), and the Fundamental Research Project of the Shenzhen Science and Technology Innovation Committee (JCYJ20210324121007020 to Z.C.).

CONFLICT OF INTEREST STATEMENT

The authors declare no conflicts of interest related to this study.

REFERENCES

1. Zhao Y, Gong Y, Liu X, et al. The experimental study of periodontal ligament stem cells derived exosomes with hydrogel accelerating bone regeneration on alveolar bone defect. *Pharmaceutics*. 2022;14:2189.
2. Jia L, Li D, Wang YN. PSAT1 positively regulates the osteogenic lineage differentiation of periodontal ligament stem cells through the ATF4/PSAT1/Akt/GSK3β/β-catenin axis. *J Transl Med*. 2023;21:70.
3. Yin S, Zhang W, Zhang Z, et al. Recent advances in scaffold design and material for vascularized tissue-engineered bone regeneration. *Adv Healthc Mater*. 2019;8:e1801433.
4. Battafarano G, Rossi M, De Martino V, et al. Strategies for bone regeneration: from graft to tissue engineering. *Int J Mol Sci*. 2021;22:1128.
5. Nuñez J, Vignoletti F, Caffesse RG, et al. Cellular therapy in periodontal regeneration. *Periodontol 2000*. 2019;79:107-116.
6. Tomokiyo A, Yoshida S, Hamano S, et al. Detection, characterization, and clinical application of mesenchymal stem cells in periodontal ligament tissue. *Stem Cells Int*. 2018; 2018:5450768.
7. Zong C, Van Holm W, Bronckaers A, et al. Biomimetic periodontal ligament transplantation activated by gold nanoparticles protects alveolar bone. *Adv Healthc Mater*. 2023;12:e2300328.
8. Li X, Guo W, Zha K, et al. Enrichment of CD146+ adipose-derived stem cells in combination with articular cartilage extracellular matrix scaffold promotes cartilage regeneration. *Theranostics*. 2019;9:5105-5121.
9. Ding T, Kang W, Li J, et al. An in situ tissue engineering scaffold with growth factors combining angiogenesis and osteoimmunomodulatory functions for advanced periodontal bone regeneration. *J Nanobiotechnology*. 2021;19:247.
10. Wang P, Wang W, Geng T, et al. EphrinB2 regulates osteogenic differentiation of periodontal ligament stem cells and alveolar bone defect regeneration in beagles. *J Tissue Eng*. 2019;10:2041731419894361.
11. Zhang Y, Luo W, Zheng L, et al. Efficient bone regeneration of BMP9-stimulated human periodontal ligament stem cells (hPDLSCs) in decellularized bone matrix (DBM) constructs to model maxillofacial intrabony defect repair. *Stem Cell Res Ther*. 2022;13:535.
12. Huang X, Chen H, Xie Y, et al. FoxO1 overexpression ameliorates TNF-α-induced oxidative damage and promotes osteogenesis of human periodontal ligament stem cells via antioxidant defense activation. *Stem Cells Int*. 2019;2019:2120453.
13. Zhang X, Jiang Y, Mao J, et al. Hydroxytyrosol prevents periodontitis-induced bone loss by regulating mitochondrial function and mitogen-activated protein kinase signaling of bone cells. *Free Radic Biol Med*. 2021;176:298-311.
14. Schröder K. NADPH oxidases in bone homeostasis and osteoporosis. *Free Radic Biol Med*. 2019;132:67-72.
15. Phull AR, Nasir B, Haq IU, et al. Oxidative stress, consequences and ROS mediated cellular signaling in rheumatoid arthritis. *Chem Biol Interact*. 2018;281:121-136.
16. Zhao Y, Gao J, Zhang Y, et al. Cyclosporine A promotes bone remodeling in LPS-related inflammation via inhibiting

ROS/ERK signaling: studies in vivo and in vitro. *Oxid Med Cell Longev*. 2021;2021:8836599.
17. Deng C, Zhou Q, Zhang M, et al. Bioceramic scaffolds with antioxidative functions for ROS scavenging and osteochondral regeneration. *Adv Sci (Weinh)*. 2022;9:e2105727.
18. Khalid S, Yamazaki H, Socorro M, et al. Reactive oxygen species (ROS) generation as an underlying mechanism of inorganic phosphate (Pi)-induced mineralization of osteogenic cells. *Free Radic Biol Med*. 2020;153:103-111.
19. Chen M, Li M, Wei Y, et al. ROS-activatable biomimetic interface mediates in-situ bioenergetic remodeling of osteogenic cells for osteoporotic bone repair. *Biomaterials*. 2022;291:121878.
20. Sharma S, Bhattarai S, Ara H, et al. SOD2 deficiency in cardiomyocytes defines defective mitochondrial bioenergetics as a cause of lethal dilated cardiomyopathy. *Redox Biol*. 2020;37:101740.
21. Sarsour EH, Kalen AL, Goswami PC. Manganese superoxide dismutase regulates a redox cycle within the cell cycle. *Antioxid Redox Signal*. 2014;20:1618-1627.
22. Wang Y, Branicky R, Noë A, et al. Superoxide dismutases: dual roles in controlling ROS damage and regulating ROS signaling. *J Cell Biol*. 2018;217:1915-1928.
23. Li J, Wang Z, Huang X, et al. Dynamic proteomic profiling of human periodontal ligament stem cells during osteogenic differentiation. *Stem Cell Res Ther*. 2021;12:98.
24. Yang Y, Zhang B, Yang Y, et al. PLGA containing human adipose-derived stem cell-derived extracellular vesicles accelerates the repair of alveolar bone defects via transfer of CGRP. *Oxid Med Cell Longev*. 2022;2022:4815284.
25. Gao J, Feng Z, Wang X, et al. SIRT3/SOD2 maintains osteoblast differentiation and bone formation by regulating mitochondrial stress. *Cell Death Differ*. 2018;25:229-240.
26. Schoppa AM, Chen X, Ramge JM, et al. Review commons transfer: osteoblast lineage Sod2 deficiency leads to an osteoporosis-like phenotype in mice. *Dis Model Mech*. 2022;15:049392.
27. Kobayashi K, Nojiri H, Saita Y, et al. Mitochondrial superoxide in osteocytes perturbs canalicular networks in the setting of age-related osteoporosis. *Sci Rep*. 2022;15:049392.
28. Li Q, Gao Z, Chen Y, et al. The role of mitochondria in osteogenic, adipogenic and chondrogenic differentiation of mesenchymal stem cells. *Protein Cell*. 2017;8:439-445.
29. Chen W, Chen X, Chen AC, et al. Melatonin restores the osteoporosis-impaired osteogenic potential of bone marrow mesenchymal stem cells by preserving SIRT1-mediated intracellular antioxidant properties. *Free Radic Biol Med*. 2020;146:92-106.
30. Sies H, Jones DP. Reactive oxygen species (ROS) as pleiotropic physiological signalling agents. *Nat Rev Mol Cell Biol*. 2020;21:363-383.
31. Harris IS, DeNicola GM. The complex interplay between antioxidants and ROS in cancer. *Trends Cell Biol*. 2020;30:440-451.
32. Hou Z, Wang Z, Tao Y, et al. KLF2 regulates osteoblast differentiation by targeting of Runx2. *Lab Invest*. 2019;99:271-280.
33. Komori T. Regulation of proliferation, differentiation and functions of osteoblasts by Runx2. *Int J Mol Sci*. 2019;20:1694.
34. Yu X, Shen G, Ren H, et al. TGFβ-induced factor homeobox 2 blocks osteoblastic differentiation through targeting pSmad3/HDAC4/H4ac/Runx2 axis. *J Cell Physiol*. 2019;234:21284-21293.
35. Mao D, Mi J, Pan X, et al. Galunisertib attenuates progression of trauma-induced heterotopic ossification via blockage of Smad2/3 signaling in mice. *Eur J Pharmacol*. 2022;928:175109.
36. Pan W, Zheng L, Gao J, et al. SIS3 suppresses osteoclastogenesis and ameliorates bone loss in ovariectomized mice by modulating Nox4-dependent reactive oxygen species. *Biochem Pharmacol*. 2022;195:114846.
37. Qi Y, Wang H, Chen X, et al. The role of TGF-β1/Smad3 signaling pathway and oxidative stress in the inhibition of osteoblast mineralization by copper chloride. *Environ Toxicol Pharmacol*. 2021;84:103613.
38. Gómez-Barrena E, Padilla-Eguiluz N, Rosset P, et al. Early efficacy evaluation of mesenchymal stromal cells (MSC) combined to biomaterials to treat long bone non-unions. *Injury*. 2020;51:S63-73.
39. Mao AS, Özkale B, Shah NJ, et al. Programmable microencapsulation for enhanced mesenchymal stem cell persistence and immunomodulation. *Proc Natl Acad Sci*. 2019;116:15392-15397.
40. Hofmann M, Wollert KC, Meyer GP, et al. Monitoring of bone marrow cell homing into the infarcted human myocardium. *Circulation*. 2005;111:2198-2202.
41. Wu Z, Chen G, Zhang J, et al. Treatment of myocardial infarction with gene-modified mesenchymal stem cells in a small molecular hydrogel. *Sci Rep*. 2017;7:15826.
42. Yu HY, Lee S, Ju H, et al. Intravital imaging and single cell transcriptomic analysis for engraftment of mesenchymal stem cells in an animal model of interstitial cystitis/bladder pain syndrome. *Biomaterials*. 2022;280:121277.
43. Wong JKU, Mehta A, Vũ TT, et al. Cellular modifications and biomaterial design to improve mesenchymal stem cell transplantation. *Biomater Sci*. 2023;11:4752-4773.

SUPPORTING INFORMATION

Additional supporting information can be found online in the Supporting Information section at the end of this article.

How to cite this article: Qiu W, Sun Q, Li N, et al. Superoxide dismutase 2 scavenges ROS to promote osteogenic differentiation of human periodontal ligament stem cells by regulating Smad3 in alveolar bone-defective rats. *J Periodontol*. 2023;1-14. https://doi.org/10.1002/JPER.23-0469